metals

Article

Laser Cladding of Iron Aluminide Coatings for Surface Protection in Soderberg Electrolytic Cells

Alex Fukunaga Gomes [1], Henrique Correa dos Santos [2], Roberto Seno [2], Adriano Francisco [3], Nelson Batista de Lima [4], Gisele Fabiane Costa Almeida [1,*], Luis Reis [5], Marcos Massi [1] and Antonio Augusto Couto [1]

[1] School of Engineering, Mackenzie Presbyterian University, São Paulo 01302-907, SP, Brazil; marcos.massi@mackenzie.br (M.M.); antonioaugusto.couto@mackenzie.br (A.A.C.)
[2] Companhia Brasileira de Alumínio, Alumínio 18125-000, SP, Brazil; henrique.correa@cba.com.br (H.C.d.S.); roberto.seno@cba.com.br (R.S.)
[3] HRC Laser Cladding, Piracicaba 13413-013, SP, Brazil; adriano@estudante.ufscar.br
[4] Instituto de Pesquisas Energéticas e Nucleares, São Paulo 05508-000, SP, Brazil; nblima@ipen.br
[5] IDMEC—Instituto de Engenharia Mecânica, Instituto Superior Técnico, Universidade de Lisboa, 1049-001 Lisbon, Portugal; luis.g.reis@tecnico.ulisboa.pt
* Correspondence: gisele.almeida@mackenzie.br

Abstract

In this work, iron aluminide coatings (FeAl and Fe_3Al) were developed on carbon steel substrates using the laser cladding process with mixtures of elemental iron and aluminum powders, aiming at protecting anodic pins in Soderberg electrolytic cells against oxidation and corrosion at high temperatures. These components operate under atmospheres rich in CO_2, alumina dust, and intense thermal cycles. The influence of processing parameters on the microstructure, phase formation, and mechanical properties of the coatings was investigated. X-ray diffraction confirmed the formation of the FeAl phase with a B2 ordered structure, while the expected $D0_3$ ordering in Fe_3Al was not detected, likely due to crystallographic texture effects. Microstructural analysis, optical and scanning electron microscopy, revealed dense coatings with good metallurgical bonding to the substrate and low porosity, being the conditions of 3.5 kW with 3 mm/s resulted in the best quality coatings. The FeAl coatings exhibited microhardness values of approximately 400 HV, whereas the Fe_3Al coatings showed values around 350 HV, indicating a significant improvement compared to the carbon steel substrate. These results demonstrate that laser cladding is an effective technique for producing iron aluminide coatings with potential application for corrosion and wear protection of anodic pins in Soderberg electrolytic cells.

Keywords: laser cladding; iron aluminides; intermetallic coatings; Soderberg anodes; protective coatings

Academic Editor: Hendra Hermawan

Received: 8 November 2025
Revised: 28 November 2025
Accepted: 1 December 2025
Published: 4 December 2025

Citation: Gomes, A.F.; Santos, H.C.d.; Seno, R.; Francisco, A.; Lima, N.B.d.; Almeida, G.F.C.; Reis, L.; Massi, M.; Couto, A.A. Laser Cladding of Iron Aluminide Coatings for Surface Protection in Soderberg Electrolytic Cells. *Metals* **2025**, *15*, 1337. https://doi.org/10.3390/met15121337

1. Introduction

Iron aluminides are promising materials for surface protection in aggressive environments due to their excellent oxidation resistance, mechanical strength, and thermal stability, which are attributed to the formation of a stable alumina layer.

Ordered intermetallic compounds constitute a unique class of metallic materials that form long-range ordered crystalline structures. These ordered intermetallics generally exist in relatively narrow compositional ranges with simple stoichiometric ratios and high thermal stability [1–3]. Owing to their low cost and excellent oxidation resistance, iron

aluminide intermetallic compounds have been widely studied since the 1930s, when their excellent oxidation resistance was first noted [4]. Among the aluminides of the FeAl system, FeAl and Fe_3Al have been investigated the most recently [5,6]. FeAl alloys can be described as a family of substitutional solid solution alloys that are ordered at low temperatures and disordered at high temperatures. In 1932, Bradley and Jay [7] reported the presence of two types of ordered structures, B2 (FeAl) and $D0_3$ (Fe_3Al), in binary FeAl alloys. Liu et al. [8] presented the ductile behavior of iron aluminides in dry oxygen. The reaction of Al atoms with water produces hydrogen atoms, which are responsible for the low ductility of FeAl-based intermetallic alloys in moisture-containing atmospheres. Generally, increasing the Al concentration decreases the density of materials and increases the oxide protective layer at high temperatures [4,9–11].

Historically, iron aluminide coatings have been produced by conventional methods such as diffusion aluminization, thermal spraying, sintering, dip casting, surface coating, and thermochemical techniques. However, these methods have significant limitations: high porosity, excessive thickness, low adhesion, high dilution, poor chemical homogeneity, and difficulty in precisely controlling the microstructure [10,12]. From the 1990s onwards, advanced processing techniques began to be studied, such as physical vapor deposition (PVD), chemical vapor deposition (CVD), reactive vaporization, modified pack cementation aluminization, and more recently, laser metal deposition (LMD) and laser cladding.

Laser cladding is a process by which a new layer of material is deposited on a substrate by laser melting powders deposited on a substrate to modify surface properties as well as repair and manufacture parts [13–16]. Among the above laser material processing technologies, laser cladding has attracted extensive research interest over the past 30 years. Laser cladding is a type of coating technology that uses a focused or defocused high-power laser beam to locally melt a thin surface layer of a material onto a substrate. Process parameters, such as laser power and scanning speed, are controlled to achieve the required thickness with minimal dilution of the substrate. Coverage of large areas is possible through the formation of adjacent individual tracks. Substrate melting is well controlled to complete metallurgical bonding at the interface so that substrate dilution is minimal, allowing the newly formed layer to retain the original composition and properties of the added materials.

Scientific literature shows a predominant focus on the use of conventional nickel- or cobalt-based superalloys for protective coatings [17–19]. These materials are employed due to their exceptional resistance to corrosion, heat, and creep in aggressive environments, such as those found in the aerospace, nuclear, marine, and oil and gas industries. Laser coatings of iron aluminides (FeAl) could replace or offer a lower-cost alternative for these same applications; however, the literature on them remains scarce. Abboud et al. [20] were the first to investigate in situ laser cladding of iron aluminide. The one-step process (single tracks) used by these authors provides speed and flexibility and opens the possibility of rapid prototyping. These authors also observed the growth of epitaxial columnar grains at the interface between the coated layer and the substrate, as well as equiaxed grains at the top of the layer, suggesting significant heat transfer by radiation and convection in the final phase of solidification. Bax et al. [21] studied entire coatings by employing overlapping strips. These authors reported that a five-layer sample was completely free of defects. However, the larger samples contained one or two smaller cracks.

As previously mentioned, one of the striking characteristics of iron aluminides is their excellent oxidation resistance at high temperatures due to the formation of a protective alumina layer that permits their use in aggressive environments. These properties make these iron aluminides promising as corrosion protection coatings on anode pins for Soderberg technology, as also studied by Kovrov et al. [22].

In recent years, laser cladding has advanced significantly as a promising technique for intermetallic deposition due to its ability to generate refined microstructures, low dilution, high adhesion, high cooling rate, and precise control of process parameters [14,23,24]. Recent studies have applied laser cladding to the production of FeAl, Fe_3Al, and reinforced FeAl composite coatings, demonstrating substantial improvements in microhardness, wear resistance, and thermal stability [25–27]. However, several challenges remain, such as aluminum loss through evaporation, the difficulty in obtaining single-phase B2 and $D0_3$ phases, the formation of residual stress cracks, intense crystallographic texture that hinders phase identification by XRD, and a scarcity of studies dedicated to single-phase coatings produced exclusively from elemental Fe and Al powders [22].

Given the properties of iron aluminides, the objective of this work is to investigate the possibility of producing single-phase coatings of iron aluminides (FeAl and Fe_3Al) on carbon steel substrates via laser cladding via mixtures of elemental iron and aluminum powders. The microstructure and microhardness profile of the deposited layers were characterized.

2. Materials and Methods

Low-carbon steel bars (AISI 1020) with dimensions of 50 mm × 150 mm × 10 mm were used as substrates for depositing iron aluminides. Before the laser coating process, the surfaces of the bars were cleaned with alcohol. Aluminum (Al, 98.7% purity) and iron (Fe, 99% purity) powders, purchased from Höganäs (Höganäs, Zweden), were used. The powders were classified by a set of vibrating sieves to ensure a particle size in the range of 70 μm to 150 μm. The morphology of the precursor powders was characterized by Scanning Electron Microscopy (SEM) as shown in Figure 1. The aluminum and iron powders were mixed and homogenized in a stainless-steel cylindrical mixer at a speed of 3 rpm for 3 h. The mixtures were prepared with stoichiometric atomic ratios corresponding to FeAl (33 wt.% Al) and Fe_3Al (14 wt.% Al).

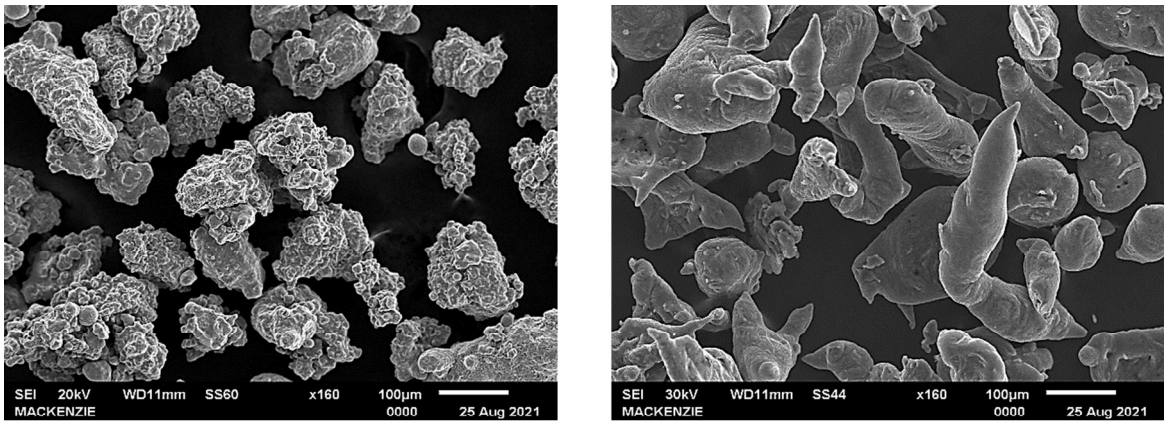

Figure 1. Images obtained by SEM of (**a**) iron and (**b**) aluminum powders used in the mixtures to obtain the tracks of iron aluminides (FeAl and Fe_3Al) via laser cladding.

The deposition process was carried out using a direct diode laser (Coherent, Luebeck, Germany) with a wavelength of 1080 nm and a Gaussian beam profile. The beam has a rectangular shape of 2 × 12 mm at the output, being guided by an optical assembly composed of a collimating lens, a focusing lens, and a shielding lens. The laser output power was adjusted on the equipment's control panel and confirmed by the internal optical monitoring system calibrated by the manufacturer. The process was conducted under a

controlled atmosphere, using 99.999% Argon inert gas as both a shielding gas and a carrier gas for the powder, ensuring stable conditions during fusion and minimizing aluminum oxidation. Deposition was performed by laser incidence onto a powder bed. Figure 2 shows the device used to standardize the deposition of the powder mixture before laser cladding. It consists of a metal plate with a rectangular groove (100 mm × 7 mm × 2 mm), in which the powder was uniformly distributed to ensure constant volume and reproducible conditions in all tracks analyzed.

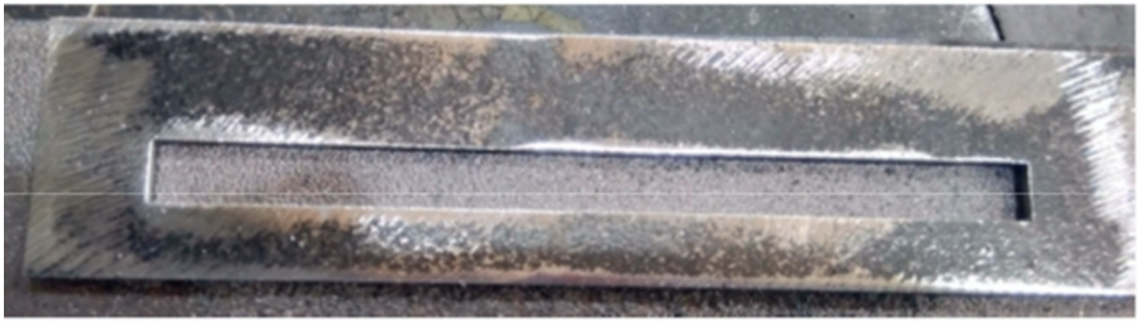

Figure 2. Device used for standardized deposition of a mixture of iron and aluminum powders to obtain iron aluminide (FeAl and Fe_3Al) tracks via laser cladding.

The process was carried out under the power and scan speed conditions provided in Table 1 (Tracks 1 and 2 were used only for equipment testing). The laser power was limited due to the risk of damage to the equipment lenses caused by the high reactivity of the aluminum powder.

Table 1. Power and scanning speed values used to obtain the tracks of iron aluminides (FeAl and Fe_3Al) via laser cladding.

Track	Aluminides	Output (kW)	Scan Speed (mm/s)
3	Fe_3Al	3.5	3
4	Fe_3Al	3.5	3
5	FeAl	3.5	3
6	FeAl	3.5	3
7	Fe_3Al	4.5	3
8	Fe_3Al	5.5	3
9	Fe_3Al	6.5	3
10	FeAl	4.5	3
11	FeAl	5.5	3
12	FeAl	6.5	3

The samples were sectioned transversely (perpendicular to the laser scan direction) for metallographic analysis. The samples were sanded and polished with a colloidal silica suspension. Next, they were subjected to chemical attack with a solution of 40 mL of HNO_3, 60 mL of CH_3COOH, and 20 mL of HCl, applied by immersion for 5–10 s at room temperature, according to procedures usually employed for the microstructural revelation of Fe–Al based coatings.

Microstructural analysis was performed on an OLYMPUS BX60 microscope (Tokyo, Japan) coupled to an image capture analyzer. SEM observations were made on a Jeol JSM-6510 microscope (Tokyo, Japan). This equipment is coupled to a Thermo Scientific Ultra Dry Energy Dispersive X-ray Spectroscopy (EDS) detector (Waltham, MA, USA) for chemical composition analysis. Vickers microhardness measurements were performed on

an Emco-test DuraScan 70 automatic tester (Zwick Roell, Ulm, Germany). A load of 1 N was applied for 10 s.

The phases present in the coatings were identified using a X-ray diffraction Rigaku Dmax instrument (Tokyo, Japan) with Cu-Kα radiation (λ = 1.5406 Å), with a scan speed of 0.02°/s, and an angular range (2θ) from 10–80°.

3. Results

A laser was applied to the mixture of iron and aluminum powders, employing simple tracks with various powder compositions, laser powers, and scanning speeds, as shown in Figure 3. Most tracks deposited by the laser cladding process were free of cracks. However, in some depositions, cracks were observed along the entire thickness of the layer. In addition, the surfaces of the deposited layers were oxidized, resulting in the formation of alumina (Al_2O_3). However, slight sanding indicated that the material below the oxide layer was completely metallic and free of any oxides. The cross-section of one of the tracks, as observed via SEM in Figure 4, displayed deposition regions of the iron aluminide, the heat-affected zone, and the substrate. The height in the central region of the coating was approximately 800 μm, and the depth of the heat-affected zone was approximately 1.65 mm. The next section contains the results and discussion of the analyses performed on the laser cladding coatings in the two compositions of iron aluminides: FeAl (33 wt.% Al) and Fe_3Al (14 wt.% Al).

Figure 3. Images of iron aluminide tracks deposited via laser cladding: (**a**) Fe_3Al track 4 and (**b**) FeAl track 6.

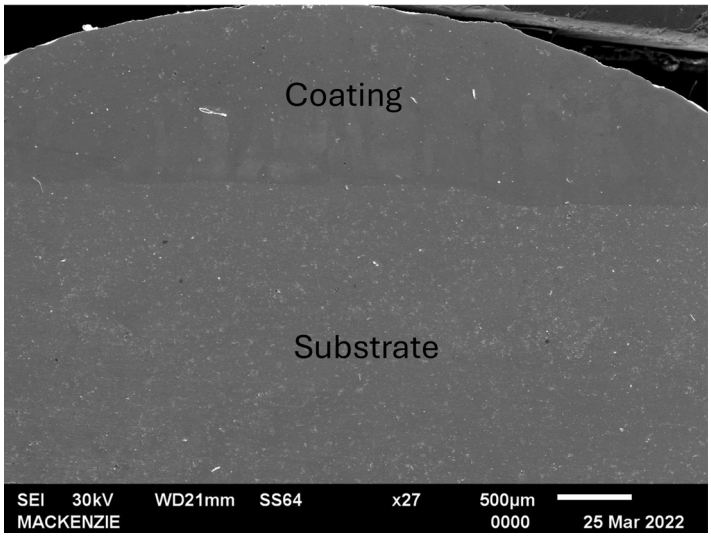

Figure 4. Cross-sectional SEM micrograph of the iron aluminide coating deposited by laser cladding, illustrating the coating–substrate interface in track 4.

3.1. Microstructure Characterization

Figure 5 shows a micrograph obtained by optical microscopy of track 4 with a FeAl composition. Note the presence of columnar grains from the interface region with the substrate and that no secondary phase appears in the cross-section. After laser fusion of the powder mixture, the grains solidified directionally from the substrate. According to Song et al. [28], columnar grain growth from a substrate can be attributed to the temperature gradient in this region. This solidification may have generated a crystallographic texture consistent with the nonappearance of some diffraction peaks of the Fe_3Al phase, which was also proposed by Bax et al. [21]. The region farthest from the substrate, near the top of the trail, presented a microstructure with equiaxed grains. Variation in the grain size and shape was expected and occurred due to variation in the cooling rate from the surface to the molten zone core. This finding agrees with that observed by Sharma et al. [29]. The optical microscopy micrographs of the other tracks (7, 8, and 9) with higher powers (4.5, 5.5, and 6.5 kW) revealed microstructures similar to those observed in tracks 3 and 4.

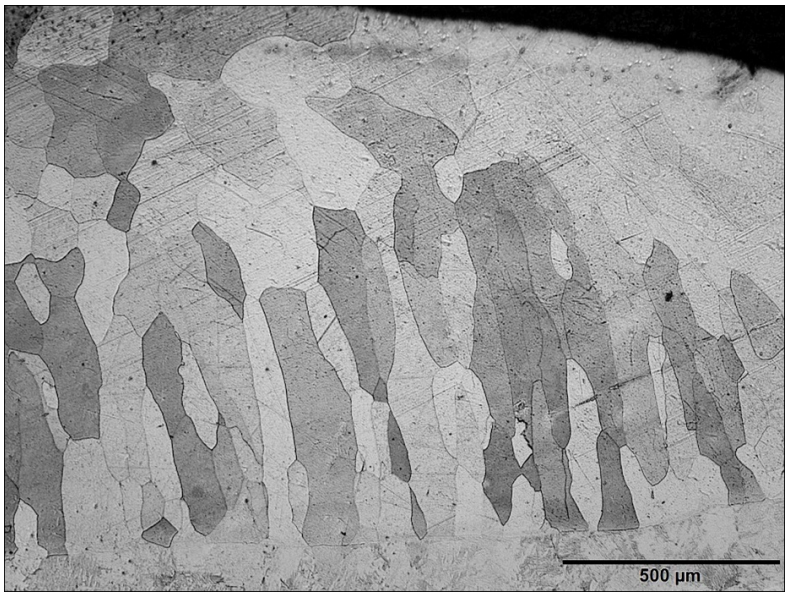

Figure 5. Micrograph obtained by optical microscopy of track 4 with an Fe_3Al composition, showing the presence of columnar grains from the interface region with the substrate.

Figure 6 shows a micrograph of the laser cladding region of Fe_3Al in track 4 observed via SEM, with the corresponding image obtained with the aluminum standard. The uniform distribution of aluminum within the coating confirmed the absence of a second phase. The chemical analysis of the aluminum content at five points from the top of the layer to near its interface with the substrate revealed values very close to each other, with an average aluminum content of 12.6 wt.% (23 at.%). A small loss of aluminum in the powder (14 wt.%) occurred due to laser melting. This slight loss of aluminum that occurred in the two compositions studied was also reported by Abboud et al. [20] and Chen & Wang [30], who attribute this phenomenon to the high reactivity and volatilization of aluminum during localized laser heating. This analysis could also not decisively verify the formation of the crystalline structure $D0_3$. However, some of the aluminum was lost during the process. Chen and Wang [12,30] reported that phase $D0_3$ could be suppressed because of aluminum dilution in the substrate and rapid solidification. According to Zhong and Liu [14], the high cooling rates achieved by laser cladding (103 to 105 K/s) imply that the ordered structure $D0_3$ would not necessarily be present at room temperature. Analysis by

X-ray diffractometry and determination of the chemical composition were not sufficient to determine the existence of this phase.

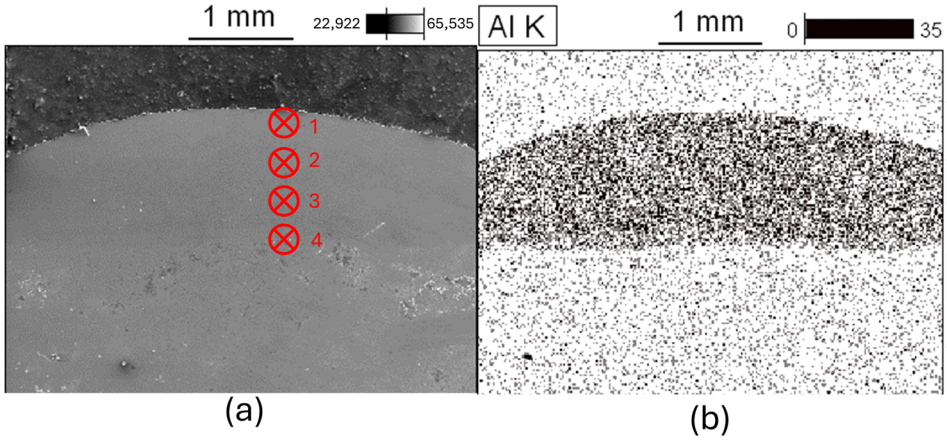

Point	Fe (at%)	Al (at%)
1	75.81	24.19
2	72.97	27.03
3	74.25	25.75
4	73.57	26.43

Figure 6. (**a**) Scanning electron microscopy (SEM) image of the region coated with laser cladding on track 4 of Fe_3Al. (**b**) SEM image obtained with the aluminum standard via energy dispersive spectroscopy (EDS).

Figure 7a shows a micrograph of the laser cladding region of FeAl on track 6 observed by scanning electron microscopy (SEM). This uniform distribution of aluminum within the coating confirms the absence of a second phase. The chemical analysis of the aluminum content at five points from the top of the layer to near its interface with the substrate revealed values very close to each other, with an average aluminum content of 29.1 wt.% (46 at.%). Like for the alloy with Fe_3Al stoichiometry, there was a small loss of aluminum in relation to the amount of aluminum prepared in the powder (33 wt.%) due to laser melting. Figure 7b shows a micrograph obtained by optical microscopy of track 6 with the FeAl composition. This figure shows an enlarged region of the track presented in Figure 7a. This micrograph shows the presence of columnar grains from the interface region with the substrate and equiaxed grains in the region closest to the top of the deposited track. As previously mentioned, in the track deposited in the Fe_3Al composition, the grains solidified directionally from the substrate because of the temperature gradient in this region. The region farthest from the substrate, near the top of the track, presented a microstructure with equiaxed grains of smaller size.

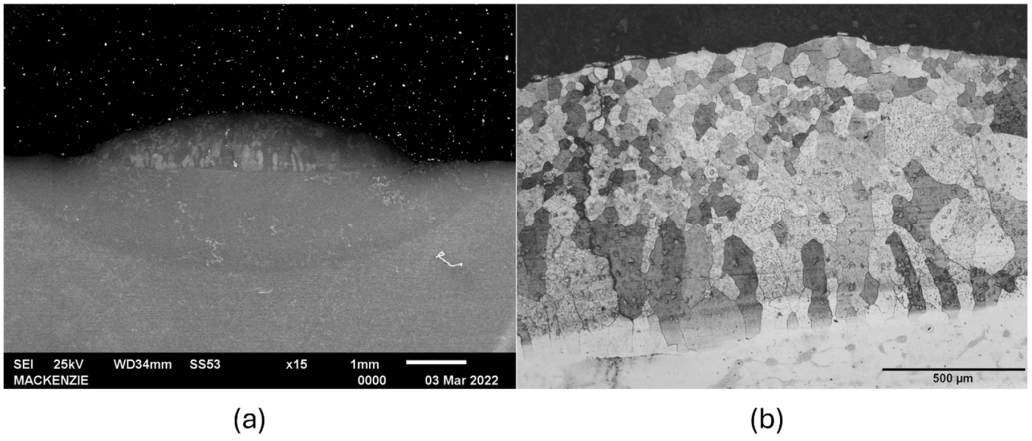

Figure 7. Micrograph of the laser-cladded region of track 6 (FeAl) observed by (**a**) scanning electron microscopy (SEM) and (**b**) optical microscopy, showing columnar grains near the substrate interface and equiaxed grains in the upper part of the deposited track.

Similarly to the tracks with different Fe_3Al compositions, the variation in grain size and shape occurred due to the varying cooling rates from the surface to the molten zone core, corroborating the findings of Sharma et al. [29] and Song et al. [28]. According to Abboud et al. [20], columnar grains grow epitaxially at the interfaces between the coating layer and the substrate, and the presence of equiaxed grains at the top of the layer suggests significant heat transfer by radiation and convection in the final stage of solidification. The optical micrographs of the other tracks (10, 11, and 12) with higher powers (4.5, 5.5, and 6.5 kW) exhibit microstructures similar to those of track 6. A crack that runs through the entire thickness of the trail is also visible in the center of this image. Cracks rarely occur in some of the deposited tracks for unidentified causes. Bax et al. [21] also reported the presence of cracks in the coating. Furthermore, these authors observed detached coatings on the substrate in most cases. This detachment of the coating was not found in the present work under any condition of deposition by laser cladding. Among the conditions evaluated, a power of 3.5 kW associated with a speed of 3 mm/s resulted in the best quality coatings with a more homogeneous microstructure and formation of intermetallic phases, free from cracks. A laser power of 6.5 kW and a scanning speed of 3 mm/s is the best combination to obtain a higher degree of B2 ordering. However, under these conditions, the contraction during cooling from higher temperatures is greater, making the coating more susceptible to cracking.

3.2. XRD Analysis

Figure 8 shows the X-ray diffractogram of the laser cladding of track 3 with an Fe_3Al stoichiometry of 3.5 kW and a velocity of 3 mm/s. This diffractogram indicates the presence of the most intense peak generated from the diffraction of the (110) plane of Fe-α with a cubic crystal structure with aluminum in a solid solution, identified using PDF card 06-0696. At this same angle, the diffraction of the (220) plane of Fe_3Al with an ordered crystalline structure D03 can occur, corresponding to PDF card 33-0397. This figure also includes the characteristic diffraction positions of planes (111) and (200) of Fe_3Al, with a $D0_3$-type ordered structure, whose peaks do not appear. This does not mean that the ordered phase Fe_3Al has not formed. The relative intensities of peaks (111) and (200) of Fe_3Al are low, and the grains may still have preferential orientations in directions that do not favor the diffraction of these planes. According to Bax et al. [21], the laser cladding of iron aluminides induces a sharp cube-like texture, with the plane (100) parallel to the surface.

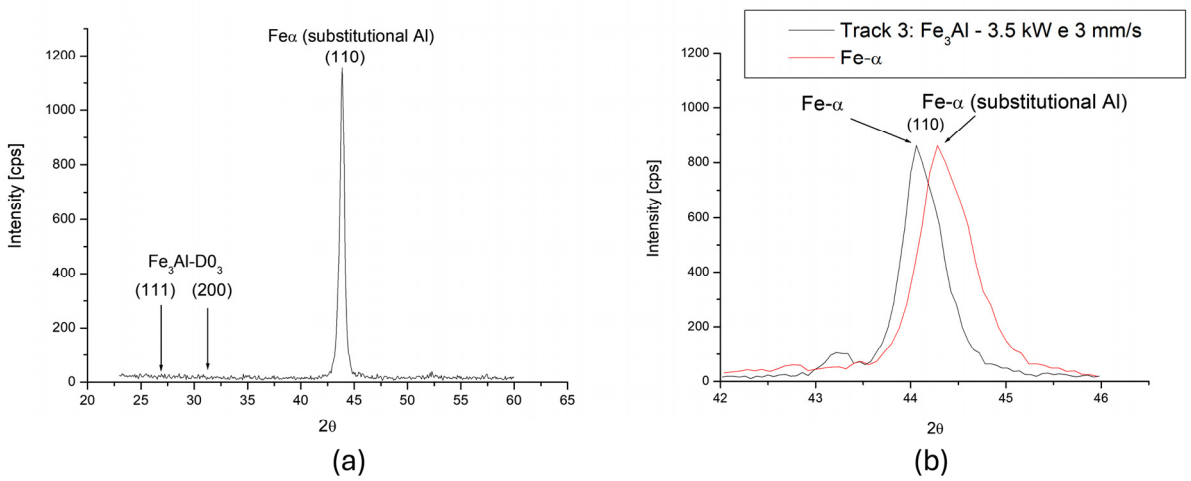

Figure 8. X-ray diffractogram of the laser cladding of track 3 with Fe_3Al stoichiometry, a power of 3.5 kW, and a scanning speed of 3 mm/s: (**a**) complete and (**b**) detailed at an angle 2θ close to the position of the peak (110).

The details in Figure 8b compare the position of the peak for the (110) plane of the solid solution α in the diffractogram of track 3 with the diffraction pattern of Fe-α, which illustrates a shift in its position at 2θ from 44.7° to 44.2°. The diffraction angle due to aluminum in the substitutional solid solution in the central cubic crosslink of iron increases the lattice parameter from 0.286 to 0.289 nm. In the formation of the ordered structure $D0_3$, the lattice parameter calculated from the position of the peak (110) is 0.578 nm. Although aluminum is in a solid substitutional solution in iron, X-ray diffractometry analysis could not verify the presence of the ordered phase $D0_3$ in Fe_3Al. The X-ray diffraction results for track 4 were similar to those for track 3. From these claddings, a speed of 3 mm/s was adopted for all the experiments to ensure a more homogeneous coating. The increase in laser power to 4.5, 5.5, and 6.5 kW in the fusion of tracks 7, 8, and 9, respectively, did not change the appearance and position of the peaks in the X-ray diffractograms from those observed in track 3.

Figure 9 shows the X-ray diffractogram of the laser cladding of track 6 with an FeAl stoichiometry of 3.5 kW and 3 mm/s. This diffractogram shows the presence of the most intense peak generated from the diffraction of the (110) plane of Fe-α with a cubic crystal structure with aluminum in the solid solution. As observed in the tracks with different Fe_3Al stoichiometries, the diffraction peak of the (110) plane of Fe-α presents a displacement due to the aluminum in the solid solution. In addition to this peak, a peak at 2θ = 31.28° occurred due to the diffraction of the (100) plane of the ordered simple cubic crystal structure B2. The presence of the peak corresponding to the diffraction of the (100) plane indicates the formation of the ordered structure B2. The absence of peaks (111), (210), and (211) in the diffraction pattern may be caused by the crystallographic texture. The FeAl-B2 phase was also identified by Sharma et al. [29], with a network parameter calculated from the peak position (220) of 0.2876 nm. According to those authors, the presence of the peak (100) in the X-ray diffraction pattern and the high hardness values obtained exclude the existence of single-phase Fe-α within the coating. According to Bax et al. [21], the FeAl-B2 phase has an accentuated cube-type crystallographic texture (preferred orientation) with the plane {h00} parallel to the surface, favoring the appearance of the diffraction peak of the plane (100).

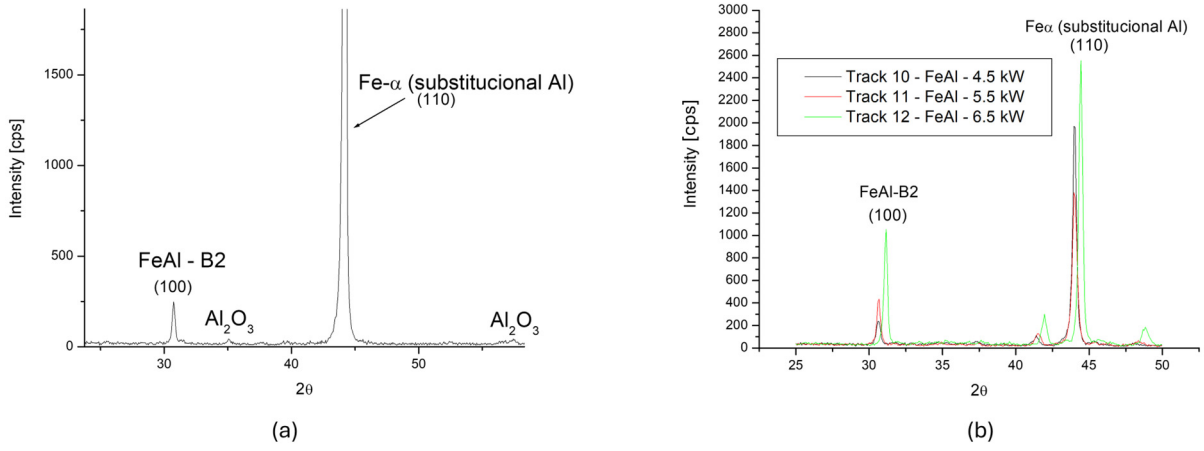

Figure 9. X-ray diffractogram of the laser cladding with FeAl stoichiometry for (**a**) track 6 (3.5 kW) and (**b**) tracks 10, 11, and 12, highlighting the relative increase in the intensity of the peak (100) of the ordered phase B2 compared with the peak (110) of Fe-α.

The X-ray diffraction results of tracks 5, 10, 11, and 12 were similar to those of track 6. Increasing the laser power to 4.5, 5.5, and 6.5 kW in the fusion of tracks 10, 11, and 12, respectively, increased the diffracted intensity of the plane (100), indicating that the degree

of order B2 increased with increasing laser power, a behavior widely reported in recent studies [23,25]. Figure 9b shows the relative increase in the intensity of peak (100) of the ordered phase B2 relative to peak (110) of Fe-α. The ratio of peak intensities differs from those in the powder diffraction file, which indicates that the coating has a preferential orientation. These diffractograms also display peaks indicating the presence of residual alumina (Al_2O_3) on the surface of the track. As previously mentioned, light sanding of the surface is sufficient to strip this oxide layer.

The increasing intensity of this peak with increasing laser power also converges with that observed by Song et al. [28], suggesting that higher energies promote greater atomic mobility and favor ordering. In contrast, for Fe_3Al, the $D0_3$ structure was not directly detected via XRD, although microhardness values indicate its presence. This result partially diverges from et al. [24], who reported explicit detection of the $D0_3$ phase, but is aligned with Bax et al. [21], who demonstrate that intense texture can suppress characteristic peaks of this phase. Thus, the results indicate that laser cladding favors the formation of ordered phases, but identification via XRD strongly depends on the crystallographic orientation induced by the process.

The results obtained in this study show strong preferential orientation in both FeAl and Fe_3Al tracks, evidenced by the disappearance or significant reduction in expected peaks in the XRD patterns. This observation is consistent with the results of Bax et al. [21] and Sharma et al. [29], who report that iron aluminide coatings produced by laser cladding tend to exhibit a cube-like texture, with {100} planes parallel to the surface. In the case of Fe_3Al, the absence of the (111) and (200) peaks of the $D0_3$ phase is consistent with the literature, which attributes this behavior to directional solidification and the rapid cooling imposed by the process. However, unlike some studies that report multiple families of preferential orientation, the samples produced in this study presented a more pronounced and homogeneous texture, possibly due to the use of the standardized powder groove, which ensures greater thermal uniformity during melting.

3.3. Microhardness

Figure 10 shows the typical microhardness profile of the substrate and the Fe_3Al composition tracks. Coordinate 0 (zero) is the interface between the substrate and the layer deposited by laser cladding from the melting of iron and aluminum powders in the stoichiometric composition of Fe_3Al. The negative distance represents the penetration in to the substrate, and the positive distance corresponds to the depth in the coating above the interface. The hardness of the deposited layer is different from that of the substrate (low-carbon steel). The higher microhardness in the coating at approximately HV0.1 = 350 indicates the possible presence of an intermetallic phase with an ordered structure $D0_3$. According to Bax et al. [21], high hardness values exclude the existence of single-phase Fe-α within the coating. According to these authors, the texture may have caused the absence of the characteristic peaks of the ordered structure $D0_3$ in the diffraction pattern.

The hardness of the deposited layer is different from that of the substrate (low-carbon steel). The higher microhardness in the coating at approximately HV0.1 = 400 indicates the possible presence of an intermetallic phase with an ordered structure B2. According to Bax et al. [21], higher hardness values confirm the existence of the ordered phase FeAl-B2.

The microhardness profiles obtained show values consistent with those reported for similar coatings in recent studies [23,27]. It was also observed that the tracks produced with higher laser power exhibited more uniform microhardness, indicating less solidified heterogeneity. This behavior converges with the literature on laser cladding of intermetallics, which demonstrates that higher energy input rates favor more homogeneous microstructures. However, unlike some studies that report a reduction in hardness due to

excessive substrate dilution, in the present study the values remained stable, suggesting that controlling the powder bed thickness was effective in minimizing dilution.

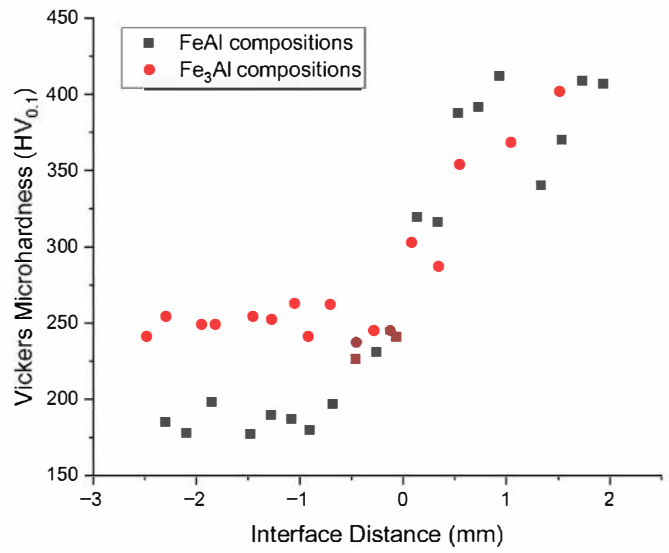

Figure 10. Typical microhardness profile of the substrate and iron aluminide tracks with FeAl (track 6) and Fe_3Al (track 4) compositions. The coordinate 0 (zero) corresponds to the interface between the substrate and the deposited layer.

4. Conclusions

This study evaluated the obtaining of single-phase coatings of iron aluminides FeAl and Fe_3Al on a carbon steel substrate via laser cladding using elemental powder mixtures. Based on the detailed microstructural characterization and evaluation of the mechanical properties, the following is concluded:

- X-ray diffraction analysis of the iron aluminide Fe3Al track revealed a shift in the peak (110) position at 2θ from 44.7° to 44.2°, indicating the presence of aluminum in the solid Fe-α solution, which was homogeneously distributed. However, the presence of the ordered D03 phase in Fe3Al was not directly identified with X-ray diffractometry analysis a fact attributed to the strong crystallographic texture generated by rapid solidification, its presence is strongly indicated by the microhardness values achieved (approximately 350 HV0.1), distinct from the substrate.
- The micrograph of the Fe3Al iron aluminide tracks shows the presence of columnar grains from the interface region with the substrate, driven by the local temperature gradient, without the precipitation of secondary phase in the cross-section. This solidification condition may have generated a crystallographic texture consistent with the nonappearance of some diffraction peaks of the ordered D03 phase in Fe3Al.
- X-ray diffraction analysis of the FeAl iron aluminides revealed the presence of the ordered structure B2. An increase in the laser power to 4.5, 5.5, and 6.5 kW in the fusion of the tracks increased the diffraction intensity of the (100) plane. This indicated that the higher heat inputs favor a great degree of ordering of the B2 structure. The grain morphology exhibited typical behavior, with columnar grains at the interface with the substrate and equiaxed grains in the upper region of the track. The average microhardness of ~400 HV0.1 confirms the obtaining of the B2 intermetallic phase.
- At 3.5 kW and 3 mm/s, coatings showed homogeneous microstructure and crack-free intermetallic phases, while 6.5 kW at the same speed promoted higher B2 ordering but increased susceptibility to cracking due to greater thermal contraction.

- The coatings produced demonstrated promising potential for application in anodic pins of Soderberg-type electrolytic cells, combining high hardness and microstructural stability. For industrial validation, it is recommended to carry out complementary corrosion, oxidation, adhesion and wear tests. As only small tracks were tested in this work, future studies should address automated deposition and detailed coating thickness measurements.

Author Contributions: Conceptualization, A.F.G., M.M. and A.A.C.; methodology, A.F.G. and A.A.C.; validation, H.C.d.S., A.F., N.B.d.L. and L.R.; formal analysis, A.F.G. and N.B.d.L.; investigation, A.F.G., H.C.d.S., R.S., N.B.d.L. and G.F.C.A.; resources, H.C.d.S., R.S., A.F. and M.M.; data curation, H.C.d.S., R.S., A.F. and L.R.; writing—original draft preparation, G.F.C.A., N.B.d.L., L.R. and A.A.C.; writing—review and editing, G.F.C.A.; visualization, R.S., A.F., L.R. and G.F.C.A.; supervision, A.A.C.; project administration, M.M. and A.A.C.; funding acquisition, M.M. and A.A.C. All authors have read and agreed to the published version of the manuscript.

Funding: This research was funded by the National Council for Scientific and Technological Development (CNPq), grant numbers 407050/2023-0 and 306559/2024-2. The doctoral scholarship awarded to the student Alex Fukunaga Gomes was supported by CNPq under the MAI/DAI 2020 program. This study also received funding from MackPesquisa, project number 251031. The author Luís Reis acknowledges the financial support of the Fundação para a Ciência e a Tecnologia (FCT) through LAETA, project UID/50022/2025 (https://doi.org/10.54499/UID/50022/2025). The APC was funded by MackPesquisa.

Data Availability Statement: The original contributions presented in this study are included in the article. Further inquiries can be directed to the corresponding author.

Acknowledgments: The authors would like to thank the National Council for Scientific and Technological Development (CNPq) for granting a doctoral scholarship to the student Alex Fukunaga Gomes under the MAI/DAI 2020 program, as well as for supporting this research through projects CNPq 407050/2023-0 and 306559/2024-2. The authors also acknowledge MackPesquisa for funding this study under project number 251031. In addition, the authors express their gratitude to the Brazilian Aluminum Company (CBA) for its partnership in this research and to HRC-Metallization for carrying out the laser cladding coatings.

Conflicts of Interest: Authors Henrique Correa dos Santos and Roberto Seno were employed by the company Companhia Brasileira de Alumínio. Author Adriano Francisco was employed by the company HRC Laser Cladding. The remaining authors declare that the research was conducted in the absence of any commercial or financial relationships that could be construed as a potential conflict of interest.

References

1. American Society for Metals. *ASM Handbook: Properties and Selection: Nonferrous Alloys and Special-Purpose Materials*; ASM International: Novelty, OH, USA, 2001; Volume 2, ISBN 0871700077.
2. Couto, A.A. *Influência Do Teor de Cromo e de Tratamentos Térmicos Na Microestrutura e No Comportamento Mecânico de Ligas Intermetálicas Ordenadas à Base de Fe3Al*; University of São Paulo: Sao Paulo, Brazil, 1998.
3. Ferreira, P.I.; Couto, A.A.; de Paola, J.C.C. The Effects of Chromium Addition and Heat Treatment on the Microstructure and Tensile Properties of Fe-24Al (at.%). *Mater. Sci. Eng. A* **1995**, *192–193*, 165–169. [CrossRef]
4. Zamanzade, M.; Barnoush, A.; Motz, H. A Review on the Properties of Iron Aluminide Intermetallics. *Crystals* **2016**, *6*, 10. [CrossRef]
5. Rojacz, H.; Varga, M.; Mayrhofer, P.H. High-Temperature Abrasive Wear Behaviour of Strengthened Iron-Aluminide Laser Claddings. *Surf. Coat. Technol.* **2025**, *496*, 131585. [CrossRef]
6. Deevi, S.C. Advanced Intermetallic Iron Aluminide Coatings for High Temperature Applications. *Prog. Mater. Sci.* **2021**, *118*, 100769. [CrossRef]
7. Bradley, A.J.; Jay, A.H. The Formation of Superlattices in Alloys of Iron and Aluminium. *Proc. R. Soc. Lond. Ser. A Contain. Pap. A Math. Phys. Character* **1932**, *136*, 210–232. [CrossRef]

8. Liu, C.T.; Lee, E.H.; McKamey, C.G. An Environmental Effect as the Major Cause for Room-Temperature Embrittlement in FeAl. *Scr. Metall.* **1989**, *23*, 875–880. [CrossRef]
9. Airiskallio, E.; Nurmi, E.; Heinonen, M.H.; Väyrynen, I.J.; Kokko, K.; Ropo, M.; Punkkinen, M.P.J.; Pitkänen, H.; Alatalo, M.; Kollár, J.; et al. High Temperature Oxidation of Fe-Al and Fe-Cr-Al Alloys: The Role of Cr as a Chemically Active Element. *Corros. Sci.* **2010**, *52*, 3394–3404. [CrossRef]
10. Tortorelli, P.F.; Natesan, K. Critical Factors Affecting the High-Temperature Corrosion Performance of Iron Aluminides. *Mater. Sci. Eng. A* **1998**, *258*, 115–125. [CrossRef]
11. Syrovatka, V.L.; Umanskiy, A.P.; Yakovlieva, M.S.; Martsenyuk, I.S.; Labunets, V.F. Oxidation Resistance of Iron Aluminide Materials. *Powder Metall. Met. Ceram.* **2019**, *58*, 29–35. [CrossRef]
12. Chen, Y.; Wang, H.M. Microstructure and Wear Resistance of Laser Clad TiC Reinforced FeAl Intermetallic Matrix Composite Coatings. *Surf. Coat. Technol.* **2003**, *168*, 30–36. [CrossRef]
13. Siddiqui, A.A.; Dubey, A.K. Recent Trends in Laser Cladding and Surface Alloying. *Opt. Laser Technol.* **2021**, *134*, 106619. [CrossRef]
14. Zhong, M.; Liu, W. Laser Surface Cladding: The State of the Art and Challenges. *Proc. Inst. Mech. Eng. Part C J. Mech. Eng. Sci.* **2010**, *224*, 1041–1060. [CrossRef]
15. Vogt, S.; Göbel, M.; Fu, E. Perspectives for Conventional Coating Processes Using High-Speed Laser Cladding. *J. Manuf. Sci. Eng.* **2022**, *144*, 044501. [CrossRef]
16. Liu, H.; Zhao, Q.; Dai, Y.; Deng, B.; Lin, J. Enhancing Corrosion and Wear Resistance of Nickel–Aluminum Bronze through Laser-Cladded Amorphous-Crystalline Composite Coating. *Smart Mater. Manuf.* **2024**, *2*, 100046. [CrossRef]
17. Kumar, V.; Hariharasakthisudhan, P.; Katiyar, J.K.; Sathickbasha, K. Advancements in Laser Powder Bed Fusion Manufacturing of Alloy 718: Microstructural Insights and Mechanical Behaviours. *J. Alloys Compd.* **2025**, *1037*, 182631.
18. Thawari, N.; Gullipalli, C.; Katiyar, J.K.; Gupta, T.V.K. Effect of Multi-Layer Laser Cladding of Stellite 6 and Inconel 718 Materials on Clad Geometry, Microstructure Evolution and Mechanical Properties. *Mater. Today Commun.* **2021**, *28*, 102604. [CrossRef]
19. Thawari, N.; Gullipalli, C.; Katiyar, J.K.; Gupta, T.V.K. Influence of Buffer Layer on Surface and Tribomechanical Properties of Laser Cladded Stellite 6. *Mater. Sci. Eng. B* **2021**, *263*, 114799. [CrossRef]
20. Abboud, J.H.; Rawlings, R.D.; West, D.R.F. Functionally Graded Nickel-Aluminide and Iron-Aluminide Coatings Produced via Laser Cladding. *J. Mater. Sci.* **1995**, *30*, 5931–5938. [CrossRef]
21. Bax, B.; Schäfer, M.; Pauly, C.; Mücklich, F. Coating and Prototyping of Single-Phase Iron Aluminide by Laser Cladding. *Surf. Coat. Technol.* **2013**, *235*, 773–777. [CrossRef]
22. Kovrov, V.; Zaikov, Y.; Tsvetov, V.; Shtefanyuk, Y.; Pingin, V.; Golubev, M. Aluminide Coating Application for Protection of Anodic Current-Supplying Pins in Soderberg Electrolytic Cell for Aluminium Production. *Mater. Sci. Forum* **2017**, *900*, 141–145. [CrossRef]
23. Wang, Y.; Feng, Y.; Sun, X.; Liu, S.; Chen, G. Effect of Process Parameters on the Microstructure and Wear Resistance of Fe_3Al/Cr_3C_2 Composites. *Coatings* **2024**, *14*, 384. [CrossRef]
24. Rajaei, H.; Amirabdollahian, S.; Menapace, C.; Straffelini, G.; Gialanella, S. Microstructure and Wear Resistance of Fe_3Al Coating on Grey Cast Iron Prepared via Direct Energy Deposition. *Lubricants* **2023**, *11*, 477. [CrossRef]
25. Chen, B.; Zhang, B.; Zhao, D.; Gao, P.; Naumov, A.; Li, Q.; Li, F.; Yang, Z.; Guo, Y.; Li, J.; et al. Microstructure and Properties of FeAlC-x(WC-Co) Composite Coating Prepared through Plasma Transfer Arc Cladding. *Coatings* **2024**, *14*, 128. [CrossRef]
26. Xia, X.; Zhang, E.; Ding, J.; Wang, Y.; Liu, Y. Research Progress on Laser Cladding of Refractory High-Entropy Alloy Coatings. *Jinshu Xuebao/Acta Metall. Sin.* **2025**, *61*, 59–76. [CrossRef]
27. Ostolaza, M.; Zabala, A.; Arrizubieta, J.I.; Llavori, I.; Otegi, N.; Lamikiz, A. High-Temperature Tribological Performance of Functionally Graded Stellite 6/WC Metal Matrix Composite Coatings Manufactured by Laser-Directed Energy Deposition. *Friction* **2024**, *12*, 522–538. [CrossRef]
28. Song, B.; Dong, S.; Coddet, P.; Liao, H.; Coddet, C. Fabrication and Microstructure Characterization of Selective Laser-melted FeAl Intermetallic Parts. *Surf. Coat. Technol.* **2012**, *206*, 4704–4709. [CrossRef]
29. Sharma, G.; Awasthi, R.; Chandra, K. A Facile Route to Produce Fe–Al Intermetallic Coatings by Laser Surface Alloying. *Intermetallics* **2010**, *18*, 2124–2127. [CrossRef]
30. Chen, Y.; Wang, H.M. Growth Morphology and Mechanism of Primary TiC Carbide in Laser Clad TiC/FeAl Composite Coating. *Mater. Lett.* **2003**, *57*, 1233–1238. [CrossRef]